A THEORETICAL STUDY ON THE SUCROSE GAP TECHNIQUE AS APPLIED TO MULTICELLULAR MUSCLE PREPARATIONS

III. Methodical Errors in the Determination of Inward Currents

E. LAMMEL
Department of Physiology, D-3550 Marburg, Federal Republic of Germany

ABSTRACT The analysis of errors associated with saline-sucrose interdiffusion in sucrose gap experiments on multicellular muscle preparations described in two previous papers (Lammel, E., 1981, *Biophys. J.*, 36:533–553, 555–573) is extended to the determination of current-voltage relations that contain an activated inward current component. The membrane current-voltage (i_t-V_m) relation used in the computations was N-shaped and consisted of two components, an outward (background) current (i_{bg}) with properties of anomalous (inward-going) membrane rectification, and an inward current (i_s) resembling the slow inward current of cardiac muscle. Reconstruction of current-voltage relations, which simulate those determined experimentally, indicates that in the potential range in which the total membrane current (i_t) is outward, i_t is measured too high, whereas it is measured too low in the range of net inward current. Reversal potentials of the inward and outward components are both shifted to more negative values, that of the inward current being more affected. Simulation of the experimental approach to evaluate i_s as the difference between i_t and i_{bg} shows that errors that produce values too high for i_{bg} are partly compensated by errors that lead to values of the net inward component that are too low. The basic features of the distorting effects analyzed are independent of different assumptions made on the selectivity of the slow inward current channels. They are related to currents emerging from the sucrose compartment (local circuit as well as externally applied currents).

GLOSSARY

Parameter Values

r_o	radius of the trabecula; 0.15 mm
l_{te}	length of the trabecula section protruding into the test compartment; 0.5 mm
l_{su}	width of sucrose compartment; 1.3 mm
l_{KCl}	length of the trabecula section exposed to the KCl compartment; 0.5 mm
ρ	fractional interstitial space; 0.25
k	tortuosity factor; 0.83
P_m	permeability coefficient of the endothelial surface sheath (given here for calcium ions to allow comparison with earlier estimates [Lammel, 1981*a*]); $0.85 \cdot 10^{-4}$cm/s
L	parameter defined in Eq. 1; 0.7.

These parameter values were chosen to simulate an experimental situation appropriate to a mammalian ventricular trabecula, because the most precise information about the slow inward current in cardiac muscle available is from investigations on this preparation. Moreover, these values were chosen to be both compatible and favorable in regard to experimental reports published to this date. The aim was to analyze those errors that appeared to be inevitable rather than those resulting (additionally) from unfavorable experimental conditions. (For a case of such unfavorable conditions see Lammel, 1981*b*.)

Definition of Symbols in Membrane Current-Voltage Relations

$c_{Na,o}$	sodium concentration in the interstitial fluid spaces
$c_{Ca,o}$	calcium concentration in the interstitial fluid spaces
$c_{K,o}$	potassium concentration in the interstitial fluid spaces; all interstitial concentrations dependent on the distance along the bundle according to the concentration profile
$c_{Na,i}$	intracellular sodium concentration; 7.5 mmol/liter (Keenan and Niedergerke, 1967; Lee and Fozzard, 1975; Ellis, 1977)
$c_{Ca,i}$	intracellular calcium concentration; 10^{-7} mol/liter (e.g., Coraboeuf, 1980)
$c_{K,i}$	intracellular potassium concentration; 150 mmol/liter (Keenan and Niedergerke, 1967; Lee and Fozzard, 1975)
i_s	slow inward current per unit area of cell membrane
P_s	permeability coefficient; 10^{-6} cm s^{-1}
a_{Na}, a_{Ca}, a_m	scaling factors for i_s; 0.207, 4.6, and 4.29, respectively
V_m	membrane potential during a voltage clamp step
$V_{m,h}$	membrane potential before the voltage clamp step (holding potential)
V'	fixed charge potential; +50 mV

d_∞	steady-state activation variable at membrane potential V_m
$f_{\infty,h}$	steady-state inactivation variable at membrane potential $V_{m,h}$
V_d, V_f, K_d, K_f	empirical constants; $V_d = -23.5$ mV, $V_f = -20$ mV, $K_d = 7$ mV, $K_f = 7$ mV
R, T, F	usual meanings
i_{bg}	background current per unit area of cell membrane
$i_{K,bg}$	component of i_{bg} carried by potassium
$i_{Na,bg}$	component of i_{bg} carried by sodium
$P_{Na,bg}$	permeability coefficient for $i_{Na,bg}$.

INTRODUCTION

This paper contains a further account of distorting effects involved in the determination of current-voltage relations in multicellular muscle preparations by the sucrose gap technique. The distorting effects considered are related to the interdiffusion of saline and sucrose in the interstitial fluid spaces of such preparations. The first in this series of papers (Lammel, 1981*a*) was concerned with this diffusion process and gave equations that described interstitial concentration distributions established under various experimental conditions. In the second paper (Lammel, 1981*b*), equations of this kind were incorporated into a mathematical model dealing with electrical events that occur in heart trabeculae subjected to voltage-clamp experiments. This model was applied to analyze methodical errors inherent to the measurement of outward membrane currents. The present study extends this theoretical approach to currents that consist of both an outward and an inward component. The inward current considered is the slow inward current of cardiac muscle, which has been extensively studied by several authors (for references, see recent reviews by Reuter [1979] and McDonald [1982]). As before, the mathematical treatment was restricted to evaluating a situation that disregards time variation.

MODEL

The mathematical model employed in this study is essentially the same as that described in previous papers (Lammel, 1981*a*,*b*). Specific modifications introduced here concern (*a*) the morphological and geometrical parameters that determine the ion concentration distribution in the interstitial fluid spaces, and (*b*) the membrane current-voltage relations assumed for the model trabecula.

Morphological and Geometrical Parameters

Fig. 1 illustrates the experimental situation underlying the mathematical description. A heart trabecula (or bundle) is mounted in a three-compartment chamber perfused with physiological saline (test compartment), isotonic sucrose, and potassium chloride solution. Current from an external source is applied across the sucrose gap in order to displace the membrane potential in the test compartment from its resting level. Some time after the three different solutions are introduced into their chambers, steady diffusion fluxes will have established along the interstitial fluid spaces (of ions from the two side compartments into the sucrose section and of sucrose in the opposite directions) resulting in complex concentration distributions of the different solutes. Simplifying the geometrical structure of the trabecula as schematically shown in Fig. 1 *B* (cylindrical shape of the bundle and of the fibers; all fibers are of the same diameter), we derived general equations in the first of this series of papers (Lammel, 1981*a*) that describe these interstitial concentration distributions; i.e., equations that express the solute concentrations in different sucrose gap arrangements as functions of the axial and radial coordinates of the trabecula. A major point derived from these equations was that steady concentration distributions do not depend on the diffusion coefficient of the special solute and are characterized by a parameter L, which combines the physical constraints of the diffusion process according to

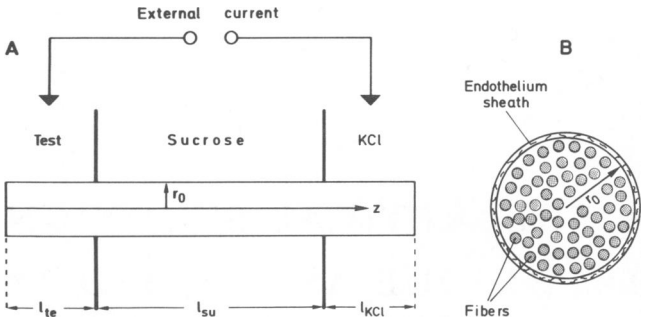

FIGURE 1 (*A*) Diagram illustrating heart trabecula in a sucrose gap chamber. r_o, radius of the trabecula; z, axial coordinate; l_{te}, l_{su}, l_{KCl}, lengths of trabecula sections exposed to test, sucrose, and KCl compartment, respectively. (*B*) Cross section illustrating the geometrical model of the trabecula.

$$L = \frac{P_m r_0}{\rho k D}. \quad (1)$$

In this definition (Eq. 16; Lammel, 1981*a*), P_m is the permeability coefficient of the endothelium cell sheath surrounding the bundle, r_0 the surface radius of the bundle, D the diffusion coefficient of the solute, ρ the fraction of cross-sectional area of the trabecula taken up by interstitial fluid spaces, and k a factor to account for the tortuosity of the diffusion pathway between the cells. (The independence of L from D results from the fact that diffusion through the surface sheath occurs via clefts between adjacent cells, and therefore P_m is proportional to D [Page and Niedergerke, 1972].)

Qualitatively, the dependence of concentration profiles on the parameters combined in Eq. 1 is as follows: radial concentration gradients of solutes diminish as L declines as a consequence of small values of both P_m and r_0. (Variations of k and ρ are of minor importance.) Axial concentration gradients also decrease with decreasing values of P_m. However, they increase with decreasing values of r_0. These effects can be intuitively understood; permeation through the surface layer becomes more and more important as a rate limiting step of solute movement into and out of the bundle as the surface permeability and/or the bundle radius decrease(s). (For more detailed information see Figs. 2 and 3 of Lammel, 1981*a*, and note that the abscissa of Fig. 3 is in terms of $z\sqrt{k}/r_0$.) It is of particular relevance that for L values of intact heart bundles commonly used in voltage-clamp experiments, radial concentration changes are small enough so that one may assume that external ion concentrations in a given cross section are the same for all fibers (see Discussion in Lammel, 1981*a*). This provides an important element of mathematical simplification, when we take into account the dependence of certain physical variables upon these concentrations as outlined in connection with Eq. 8 below.

When choosing the parameter values given in the Glossary, we made special reference to a recent study on trabeculae from cow hearts by Reuter and Scholz (1977). Following a procedure previously described (Lammel, 1981*a*), we obtained an estimate for P_m ($0.85 \cdot 10^{-4}$ cm/s) from the data of these authors (legend of their Fig. 2). They measured a series resistance (R_s) of 480 Ω and a total input capacity (C_m) of 0.81 μF for a bundle section of 0.7-mm length (l_{te}). In converting R_s into P_m, the radius (r_0) of the bundle concerned (not given by the authors) was estimated from C_m and l_{te}. Assuming a specific membrane capacity of 1

$\mu F/cm^2$, a cell radius of 8.9 μm (calculated from the average cross-sectional area of cow heart fibers determined by Marceau, 1904), a surface-to-volume ratio of 0.4 μm^{-1} (Page and McCallister, 1973), and a fractional interstitial volume (ρ) of 0.25, r_0 comes to 0.36 mm. Note that the P_m value obtained this way from R_s, l_{te}, and r_0 is in good agreement with other estimates for mammalian trabeculae of different species (Lammel, 1981*a*).

The tortuosity factor, k, was calculated from Eq. 10 of Lammel (1981*a*) based on the simplified cross-sectional structure illustrated in Fig. 1 *B*. This equation relates k to ρ according to

$$k = \left[1 + \frac{4}{\pi}(1 - \rho)\left(1 - \frac{\pi}{4}\right)\right]^{-1}. \quad (2)$$

The values for the radius and the segmental lengths were chosen for the following reasons. The radius is the smallest of the range of preparations used by Reuter and Scholz (1977). Given the other morphological data contained in the definition of L (Eq. 1), a small radius helps to achieve a steep concentration profile between sucrose and electrolyte compartments. This serves to reduce contamination of the interstitial medium of the test section by sucrose, while at the same time, the length of this section can be kept short in order to safeguard axial uniformity of the membrane potential. (Errors due to radial voltage inhomogeneity, not considered in this paper, are also reduced by choosing a small bundle radius. See Reuter and Scholz [1977] for experimental information and also Attwell and Cohen [1977] and Haas and Brommundt [1980] for a theoretical analysis of this subject.) A steep concentration profile is furthermore related to a high external resistance (assumed here to reside exclusively in the interstitial fluid spaces) between the two electrolyte chambers, and therefore to a low shunt factor. This factor, commonly used to characterize sucrose gap arrangements, is defined as the ratio of the total intracellular resistance over extracellular resistance (R_i/R_e) across the gap.

A small value of R_i/R_e is important to keep the fraction of applied current (I), which bypasses the fibers extracellularly as shunt current, low. Because (at a given radius) the shunt factor increases with decreasing width of the sucrose compartment, the value of l_{su} presents a compromise between such an intention and the need to keep this distance short in order to avoid unnecessarily long computation times. Using the parameter values listed, we compute the shunt factor of the present model arrangement as 0.085. (The procedure of calculating R_e from the ion concentration profile was described in the preceding paper [Lammel, 1981*b*].) Because of the smaller radius, this value is considerably lower than that computed for the experimental situation in Fig. 2 of Reuter and Scholz (1977) (r_0 = 0.36 mm; l_{su} = 2 mm; L ~ 1.5; R_i/R_e = 0.23). The length of the test section (l_{te}) chosen for the model is on the lower side of the range of values given by Reuter and Scholz (1977). To characterize the concentration profile, note that the average cross-sectional ion concentration in the center of this section (z = 0.25 mm) comes to 90% of the bathing fluid and decreases to a level very close to 50% at the left edge of the sucrose compartment. This value is slightly higher than the corresponding value computed for the arrangement of Fig. 2 of Reuter and Scholz (1977) (l_{te} = 0.7 mm; mean concentration at z = 0.35 mm; 87%). Finally, the value of l_{KCl} (usually not given in the literature) was chosen to provide a sufficiently large membrane area for current to enter the model trabecula.

Membrane Current-Voltage Relations

In the study selected to provide several of the parameter values for the present model, Reuter and Scholz (1977) gave a mathematical description of the calcium-dependent slow inward current (i_s) based on the constant-field theory (Goldman, 1943; Hodgkin and Katz, 1949). We adopted this as a simple and suitable approach to quantify the dependence of this current on the electrochemical gradient across the cell membrane. On the basis of their experimental results on the sensitivity of i_s to variation of external Ca and Na concentrations, Reuter and Scholz describe the conductance channel as being permeable to Ca, Na, and K ions with ratios of the permeability coefficients of P_{Ca}/P_{Na} = 100, and P_{Ca}/P_K = 100. In addition to using this interpretation, we also analyzed two cases in which i_s is either carried purely by Na or by Ca ions. The intention underlying these alternative assumptions was to evaluate the possible existence of special distorting effects that depend on the ion species carrying the inward current. This seemed interesting because the selectivity of the slow channel is a matter of intense discussion and seems to vary considerably between preparations of different origin (e.g., Coraboeuf, 1980; Hagiwara and Byerly, 1981).

Two kinds of current-voltage relations, which are frequently determined experimentally, were investigated; (*a*) relations between the membrane potential and the current at the time of the maximum of i_s and (*b*) instantaneous current-voltage relations determined after maximal activation of the conductance channel of i_s. As described below, in both cases, we computed membrane potential distributions occurring along the model trabecula at a particular time during the transient inward current. Thus, we omit time variation from the model equations in order to simplify the mathematical treatment considerably. We provide arguments to justify this restriction and to estimate related errors on the basis of present experimental knowledge in the Discussion section.

The following Eqs. (3a–c) were used alternatively to describe the slow inward current (Reuter and Scholz, 1977)

$$i_s = P_s \cdot a_{Na} \cdot d_\infty \cdot f_{\infty,h} \cdot A_{Na} \quad (3a)$$

or

$$i_s = P_s \cdot a_{Ca} \cdot d_\infty \cdot f_{\infty,h} \cdot A_{Ca} \quad (3b)$$

or

$$i_s = P_s \cdot a_m \cdot d_\infty \cdot f_{\infty,h}(A_{Ca} + 0.01A_{Na} + 0.01A_K) \quad (3c)$$

where

$$A_{Na} = \frac{(V_m - V')F^2}{RT} \cdot \frac{c_{Na,i}\exp(V'F/RT) - c_{Na,o}\exp[-(V_m - V')F/RT]}{1 - \exp[-(V_m - V')F/RT]}; \quad (4a)$$

$$A_{Ca} = \frac{4(V_m - V')F^2}{RT} \cdot \frac{c_{Ca,i}\exp(2V'F/RT) - c_{Ca,o}\exp[-2(V_m - V')F/RT]}{1 - \exp[-2(V_m - V')F/RT]}; \quad (4b)$$

$$A_K = \frac{(V_m - V')F^2}{RT} \cdot \frac{c_{K,i}\exp(V'F/RT) - c_{K,o}\exp[-(V_m - V')F/RT]}{1 - \exp[-(V_m - V')F/RT]}; \quad (4c)$$

$$d_\infty = \{1 + \exp[-(V_m - V_d)/K_d]\}^{-1}; \quad (5)$$

$$f_{\infty,h} = \{1 + \exp[(V_{m,h} - V_f)/K_f]\}^{-1}. \quad (6)$$

The meanings of the symbols used in these equations are given in the Glossary. Note that concentrations instead of activities were used. The values for P_s and the scaling factors a_{Na}, a_{Ca}, and a_m were chosen to achieve (*a*) approximate resemblance to the results of Reuter and Scholz (1977), and (*b*) identical values of the three current-voltage relations used alternatively for the peak inward current occurring with a clamp pulse to ~ −10 mV. An illustration of the different membrane current-voltage relations is given in Figs. 2 and 3 in the Results section. The equations show that it was assumed for simplicity that the faster reaction, d, which determines the activation of the slow inward current, reaches steady-state

values without any concomitant change of the inactivation variable, f (use of $V_{m,h}$ in Eq. 6).

A background current (i_{bg}) of the kind investigated in the preceding paper (Lammel, 1981*b*) was added to the slow inward current. The main component of this current was a potassium current ($i_{K,bg}$), whose permeability was assumed to exhibit anomalous (inward-going) rectification, as is characteristic for skeletal and cardiac muscle (Katz, 1949; Hodgkin and Horowicz, 1959; Hutter and Noble, 1960). This current was mathematically described according to Eqs. 9a and 10 of Lammel (1981*b*), with the minor modification that the permeability coefficient (Eq. 10) was increased by a factor of 1.2 over the entire range of membrane potential. The other component of the background current was a sodium leakage current ($i_{Na,bg}$) given by

$$i_{Na,bg} = P_{Na,bg} \cdot A_{Na}, \quad (7)$$

where $P_{Na,bg} = 10^{-8}$ cm s^{-1}, and A_{Na} is defined by Eq. 4a. An illustration of i_{bg} as a function of V_m at physiological external ion concentration is included in Fig. 2. Further alterations with regard to the preceding paper (Lammel, 1981*b*) concerned some of the other parameter values used for the computations. The following values, appropriate to mammalian preparations, were adopted: $c_{Na,T} = 149.3$ mmol/liter, $c_{Ca,T} = 1.8$ mmol/liter, $c_{K,T} = 5.4$ mmol/liter (sodium, calcium, and potassium concentrations in the test compartment, respectively; Tyrode solution); $T = 308$ K (temperature); $G_i = 0.0021\ \Omega^{-1}$ cm^{-1} (conductivity of intracellular medium, Weidmann, 1970).

Calculation of Distorting Effects from the Model

The rationale for the present approach of treating the electrical events in the model trabecula by means of the one-dimensional cable theory was described in the preceding study (Lammel, 1981*b*). To outline the procedure we followed for evaluating methodical modifications of current-voltage relations, it may suffice here to reformulate Eq. 8 of the same paper

$$\frac{d^2V_m}{dz^2} = (r_e + r_i)i_m + \frac{dr_e}{dz}\left(\frac{dV_m}{dz} + \frac{dE_e}{dz} + r_i I\right)\Big/(r_e + r_i) - \frac{d^2E_e}{dz^2}. \quad (8)$$

In this differential equation for the membrane potential V_m, r_i represents the axial intracellular resistance (i.e., the parallel internal resistance of all fibers) and r_e the extracellular resistance (i.e., the resistance residing in the interstitial fluid spaces), both per unit length of the trabecula. i_m is the membrane current per unit length of the trabecula, I the current applied to the bundle from the external current source, and E_e the liquid junction potential set up by the ionic concentration gradients within the interstitial fluid spaces.

Equations that relate E_e and r_e to the interstitial ion concentrations were given in connection with the derivation of Eq. 8 (Eqs. 11 and 13; Lammel, 1981*b*). Expressing these concentrations analytically in terms of their cross-sectional mean values (see remarks in connection with Eq. 1 for the basis of this approximation), E_e and r_e become functions of the axial coordinate z, and Eq. 8 can be solved numerically with any relation that describes i_m as a function of the membrane potential and intra- and extracellular ion concentrations. According to the usual experimental procedure, the simulation of measured current-voltage relations was performed as follows. First, i_m, in Eq. 8, was expressed in terms of one of the membrane current-voltage relations given in the last section. Eq. 8 was then solved by means of an extrapolation method with automatic stepsize correction (Bulirsch and Stoer, 1966) to obtain a membrane potential distribution ($V_m[z]$) that satisfies (*a*) special boundary conditions at either end of the model trabecula, and (*b*) continuity conditions at the two edges of the sucrose compartment for a particular value of externally applied current, I (Lammel, 1981*b* and Results section of this paper). By repeating this integration procedure several times with different values of I, we computed a family of V_m distributions depending on the individual i_m relation used. Finally, the measured current-voltage curve belonging to this i_m relation was constructed from this family of V_m distributions by plotting the different I values against the respective values of V_m (z) at the middle of the test section (clamp potentials at $z = 0.25$ mm). (For comparison with the i_m relations, I values were converted into current densities by dividing them by the membrane area exposed to the test compartment.)

A minor problem arising in connection with this was how to include $f_{\infty,h}$, the variable, which describes the degree of inactivation before the clamp pulse, into the integration procedure. This was done in the following way. In the left-hand part of the model trabecula ($0 \le z \le 1.1$ mm), the value $f_{\infty,h} = 1$ was assumed ($V_m < -50$ mV before the clamp pulse; see Fig. 13 *A* in Reuter and Scholz, 1977). In the right-hand part ($z \ge 2.1$ mm), $f_{\infty,h}$ was set equal to zero (complete inactivation because of the isotonic potassium solution in the right-hand compartment). In the intervening region ($1.1 \le z \le 2.1$ mm), $V_{m,h}$ in Eq. 6 was expressed in terms of a linear function of z: $V_{m,h} = az + b$, where $a = 0.79868$ V cm^{-1} and $b = -0.117404$ V. This function is an approximation of the resting potential distribution in this region, which is obtained simply from the background current (i.e., by integration of Eq. 8 with $i_m = i_{bg}$ and $I = 0$).

A similar problem was met in the computation of the V_m distributions carried out to simulate instantaneous current-voltage relations. In voltage clamp experiments, such relations are obtained by means of double clamp steps. The first step, of constant amplitude and duration, serves to make the membrane permeability attain a certain level. The current that is measured to obtain the instantaneous current-voltage relation is the current flowing immediately after the conditioning prepulse at the beginning of the second step. This second step is of varying amplitude, and determines the driving force (e.g., Hodgkin and Huxley, 1952*b*; Reuter and Scholz, 1977). In the present analysis, it was assumed that, by the conditioning prepulse, a state of maximal activation ($m_\infty = 1$) is reached in the test section ($V_m = +27$ mV at $z = 0.25$ mm). This state is characterized by a particular V_m distribution and thus by a particular conductance distribution of the activated channel along the model trabecula. (The V_m distribution chosen is illustrated by curve 5 of Fig. 4 *a* in the Results.) The conductance distribution established by the conditioning pulse was computed in a first integration program, and the actual values obtained at the edges of each integration step were stored. These values were then used to describe the conductance distribution analytically (by piecewise linear approximation within each integration step) in later computations of V_m distributions for the construction of instantaneous current-voltage relations. (The mathematical description of the background current, i_{bg}, in this procedure was unchanged.)

RESULTS

As outlined in the last section, the first step in applying the mathematical model to the present problem is to compute membrane potential distributions by numerical integration of Eq. 8. Before considering these distributions, however, we give an illustration of the membrane current-voltage relations introduced into the integration scheme as well as of those reconstructed as measured current-voltage relations from the computational results. Fig. 2 shows these relations for the case in which the slow inward current was assumed to be carried purely by Na ions. The membrane current-voltage relations (solid curves) represent the following. The curve labeled i_i represents the total specific membrane current determined at the peak of the slow inward current, i_s. This current is composed of i_s and the background current, i_{bg}. i_s was calculated from Eqs. 3a, 4a,

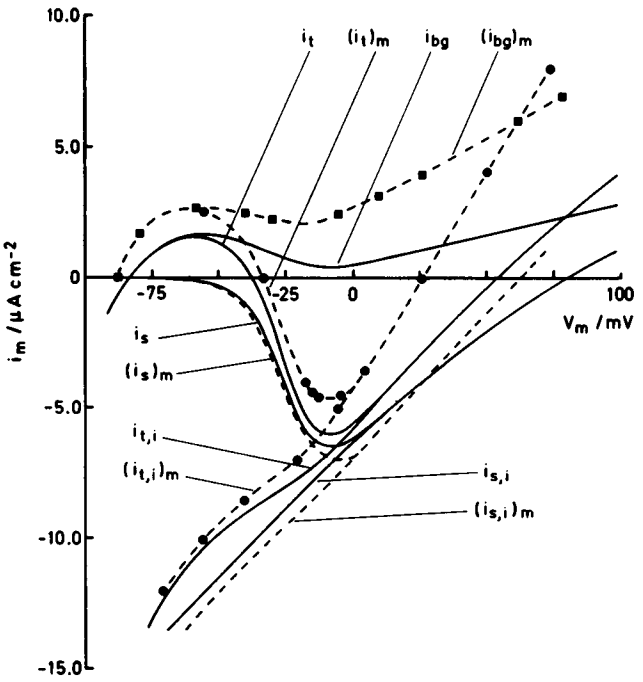

FIGURE 2 Comparison of membrane current-voltage relations assumed for the model (solid curves) with predicted measurements of current-voltage relations (dashed curves). i_s, slow inward current. The curve represents peak values of this current flowing upon stepwise change in membrane potential (V_m, abscissa). i_s is assumed to be carried by Na ions. i_{bg}, background current. i_t, total current ($i_t = i_s + i_{bg}$). Subscript i indicates instantaneous determination of current after maximal activation of the slow inward current channel; subscript m, modification due to the recording technique. Symbols represent computational results from which dashed curves were fitted by eye; ●, results based either on i_t or $i_{t,i}$, ■, results based on i_{bg}. $(i_s)_m$ is the difference between $(i_t)_m$ and $(i_{bg})_m$, $(i_{s,i})_m$ is the difference between $(i_{t,i})_m$ and $(i_{bg})_m$.

and 5 while setting $f_{\infty,h} = 1$ and $c_{Na,o} = c_{Na,T} = 149.3$ mmol/liter. Curves $i_{t,i}$ and $i_{s,i}$ represent instantaneous membrane current-voltage relations computed with $d_\infty = 1$ and $f_{\infty,h} = 1$ in Eq. 3a over the entire range of membrane potential. $i_{t,i}$ is the total membrane current and $i_{s,i}$ the component of $i_{t,i}$ that flows through the slow inward current channels ($i_{t,i} = i_{s,i} + i_{bg}$).

In regard to the reconstruction of the measured current-voltage relations (dashed curves in Fig. 2), a few remarks concerning the experimental identification of i_s become necessary. Because the excitatory sodium current (responsible for the rapid upstroke of the action potential) has a much faster time course and can be eliminated either by tetrodotoxin or by choosing a holding potential high enough to inactivate this current, the problem here is to separate i_s from outward currents normally carried by potassium ions. In a recent review on voltage-dependent calcium channels, Hagiwara and Byerly (1981) pointed out that all possible methods for separating two currents follow a slightly generalized form of a procedure as first outlined by Hodgkin and Huxley (1952*a*). The total current is measured at a particular voltage, before and after some manipulation, that changes one of the two components. Problems inherent to different approaches when using this procedure were thoroughly discussed by these authors. The approach frequently applied to cardiac muscle was to measure the total current before and after blocking the slow inward current (see recent review by Coraboeuf, 1980). Clearly, the validity of this method depends on the selectivity of the blocking substance, i.e., on its ability to eliminate i_s without changing the outward current. Although this condition is not fully satisfied by the blocking agents available at present (Hagiwara and Byerly, 1981), we simulated this experimental procedure by carrying out the following computational operations. In a first series of integrations of Eq. 8, i_m was introduced into the equation as the sum of i_s and i_{bg}. The result obtained from these computations is the curve labeled $(i_t)_m$ in Fig. 2, which represents the measured current-voltage relation belonging to i_t. In a second series of integrations, i_m in Eq. 8 was expressed in terms of i_{bg} alone. Based on these computations, the curve $(i_{bg})_m$ was constructed; it represents the outward current i_{bg} (after elimination of i_s) as modified by the recording technique. Finally, the curve $(i_s)_m$ illustrating the measured slow inward current was obtained as the difference between the curves $(i_s)_m$ and $(i_{bg})_m$. Analogously, the instantaneous relation, $(i_{s,i})_m$, was determined by first computing $(i_{t,i})_m$ and then subtracting the outward component, $(i_{bg})_m$, from this current. (The points illustrated by symbols on the curves $(i_t)_m$, $(i_{bg})_m$, and $(i_{t,i})_m$ represent the computational results that were fitted by eye. This means that each of these points was obtained from a membrane potential profile, computed with a particular value of I using the respective membrane current-voltage relation; see last section.)

Comparing the membrane current-voltage curves with those representing the measured relations, we can see that a clear resemblance exists for each pair of curves. However, differences are also apparent. A comparison of the curve $(i_t)_m$ with curve i_t, for example, shows that the resting potential is shifted by 5 mV and the positive reversal potential by 27.5 mV, both to more negative values. Furthermore, the amplitudes of this current are altered in a way indicating that the outward current is measured too high by the recording method, whereas the inward current is measured too low. It is interesting, however, that the pure inward current $(i_s)_m$, evaluated as just described, is slightly larger than i_s over a wide range of V_m, and that there is closer resemblance between these two curves.

Fig. 3 illustrates that the basic features of these distorting effects are independent of the ion species carrying i_s. The curves of Fig. 3 *Aa* are simply replots of the current-voltage relations i_t and $(i_t)_m$ of Fig. 2, while the curves of Fig. 3 *Ba* are replots of the relations i_s and $(i_s)_m$ of Fig. 2. Figs. 3 *Ab* and 3 *Bb* show current-voltage relations computed in a completely analogous way, except that the slow inward current was assumed to be carried solely by Ca ions. This means that the expression for i_s entered into the

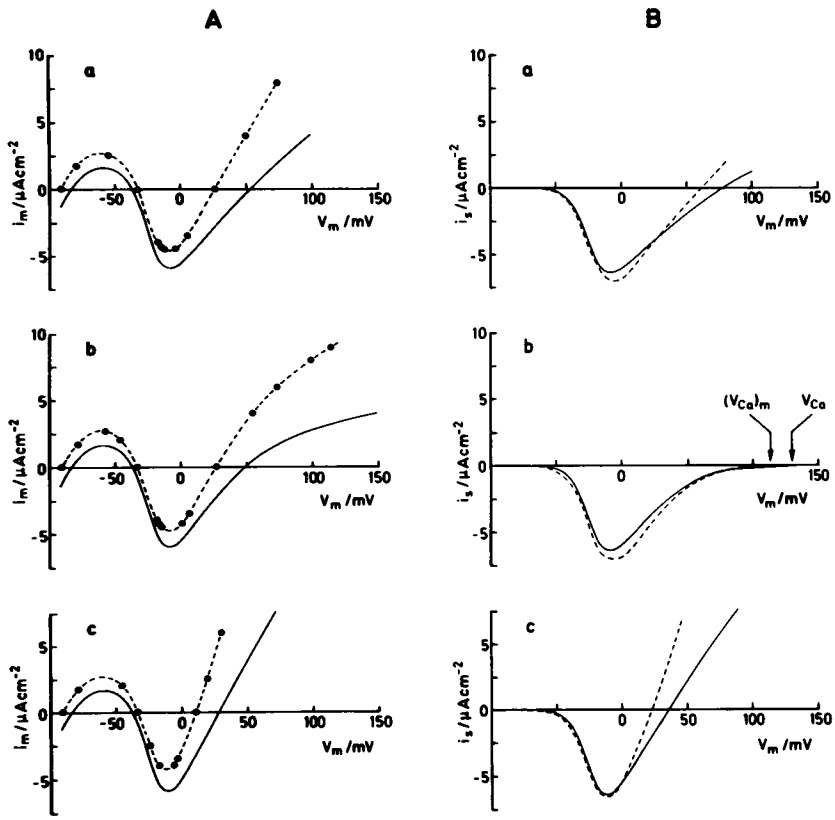

FIGURE 3 Comparison of membrane current-voltage relations (solid curves) with predicted measurements of current-voltage relations (dashed curves) for different selectivities of the conductance channel of the slow inward current (i_s). From top to bottom: (*a*) i_s carried by Na ions; left (*A*a), replot of curves i_t and $(i_t)_m$ of Fig. 2; right (*B*a), replot of curves i_s and $(i_s)_m$ of Fig. 2. (*b*) Same conditions and representation of results as in (*a*), except that i_s is assumed to be a pure Ca current. V_{Ca} in (*B*b) is the true and $(V_{Ca})_m$ the measured reversal potential of i_s. (*c*) Like (*a*), but with i_s being a mixed current carried by Ca, Na, and K ions. Relative permeabilities of the conductance channel in this case: $P_{Ca}/P_{Na} = P_{Ca}/P_K = 100$.

integration scheme was formulated according to Eq. 3b. In Figs. 3 *Ac* and *Bc* corresponding results are illustrated for the assumption that i_s is a mixed current made up by the flow of calcium, sodium, and potassium as defined in Eq. 3c. In all three cases, the background current i_{bg} and therefore the relation $(i_{bg})_m$ used to determine $(i_s)_m$ by subtraction from $(i_t)_m$ is the same as illustrated in Fig. 2. As already mentioned, distortions of this outward current were treated in detail in the preceding paper (Lammel, 1981*b*). It should be emphasized, however, that although the geometrical and morphological parameters for the model were chosen quite differently, the present results agree well with those derived previously for the case of favorable experimental conditions (Fig. 8 *A*; Lammel, 1981*b*).

The main object of the following consideration of the current and voltage distributions illustrated in Fig. 4 is to provide insight into the origin of the distorting effects. For the computation of these distributions, the i_t vs V_m relation of Fig. 2 was used in the integration scheme. To reduce the complexity of the representation, only six of the twelve distributions computed to construct the curve $(i_t)_m$ in Fig. 2 (indicated by the twelve symbols) are shown. Turning first to the membrane potential profiles (Fig. 4 a), one can see that, according to the three zero current potentials of the i_t relation, three different profiles are obtained for the value $I = 0$. Profile 1 corresponds to the resting potential, profile 3 to the zero current potential in the negative slope range, and profile 5 to the reversal potential in the positive potential range. For the other profiles, the positive sign of I defines inward direction of applied current in the test region, and the negative sign defines the outward direction.[1] A common feature of all profiles is that deflections from the resting potential extend far into the sucrose region before the membrane potential reaches the level near zero

[1]In practice, the profiles of Fig. 4 a that have to satisfy boundary conditions in terms of dV_m/dz at either end of the model trabecula [Lammel, 1981*b*] were computed as follows; the integration of Eq. 8 was started with the exact value of dV_m/dz and an estimated value of V_m at the left end of the trabecula. This V_m value was then corrected in consecutive integration runs in order to approximate the value of dV_m/dz required at the other end. In a certain range of I values, $I_1 < I < I_2$, [I_1 and I_2 defining the minimum and maximum of the N-shaped part of the curve $(i_t)_m$], this integration converges to three different V_m profiles. Outside of this range, for each value of I, exists only one profile that satisfies the boundary conditions.

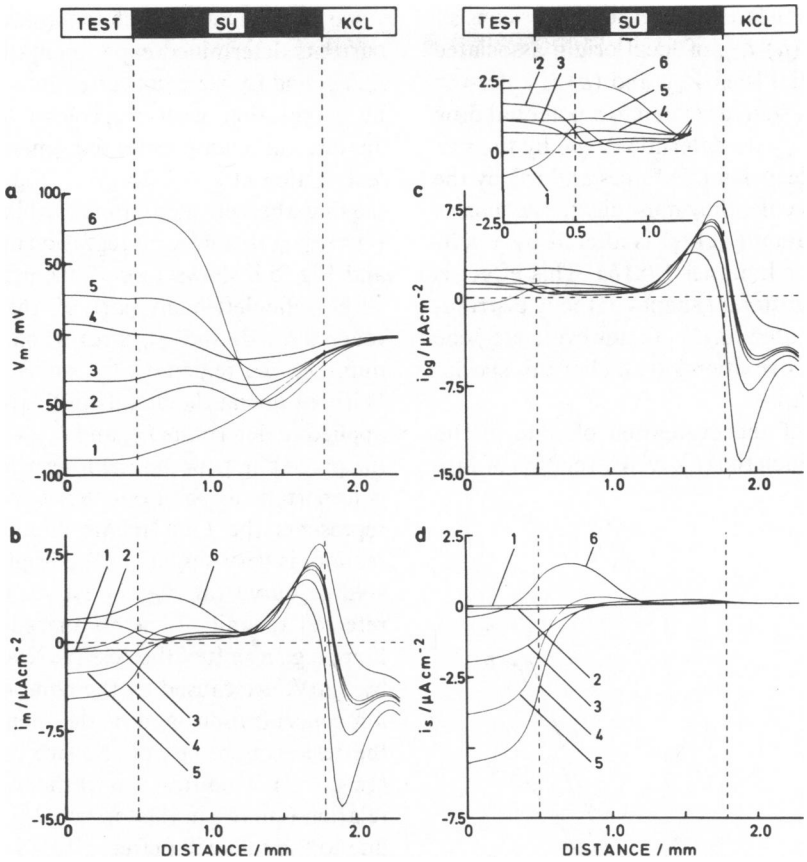

FIGURE 4 Computed distributions of membrane potential (*a*) and membrane current (*b*) along the model trabecula. Membrane current (i_m) consists of background current (i_{bg}) and slow inward current (i_s) plotted in panels *c* and *d*, respectively. *Inset* in *c*: replot of left-hand part of i_{bg} distributions on enlarged ordinate scale. Numbers at curves indicate strength of externally applied current (I). In µA: 1, $I = 0$; 2, $I = -0.25$; 3, $I = 0$; 4, $I = +0.35$; 5, $I = 0$; 6, $I = -0.8$. Lengths of preparation segments and bathing fluids in the three compartments are indicated at the top.

set up by the isotonic potassium solution in the right-hand compartment.

Compared with the membrane potential distributions, the related current profiles in the vicinity of the test-sucrose junction (Fig. 4 *b*) appear to be rather complex. Part of this complexity results from the fact that the membrane current consists of two components that both depend on the membrane potential in a nonlinear fashion. These components, i_{bg} and i_s, are separately illustrated in Figs. 4 *c* and *d*. The other more important factor, which causes the axial nonuniformity of the current distributions, is the change of ionic equilibrium potentials and conductances with the interstitial ion concentrations at the sucrose-electrolyte junctions. For the background current, this change leads to profiles quite similar in shape to those obtained in the preceding paper. (Compare Fig. 4 *c* of the present study with Fig. 5 *Ab* of Lammel [1981*b*] and note that both the computed membrane potential and the ion concentration, i.e., the two variables determining i_{bg} according to Eqs. 9 and 10 of the preceding paper, exhibit similar distributions on a different abscissa scale in the two model trabeculae.) In the case of the slow inward current (Fig. 4 *d*), note that the axial change of the external ion concentration at the test-sucrose junction is associated with a reversal of the direction of the driving force. Clearly, the position of current changing from inward to outward moves from right to left along the axis as the membrane potential is shifted in a positive direction.

Of the profiles illustrating the membrane current, i_m, profiles 1, 3, and 5 are of particular interest. Because all of them were obtained under the condition $I = 0$, they represent pure local circuit currents caused by electromotive forces present in the bundle itself; these being (*a*) the liquid junction potential, E_e, and (*b*) the ionic equilibrium potentials at the cell membrane. As is readily understood, the contribution of the ionic equilibrium potentials to the flow of these currents is because they vary spatially along the bundle axis. The occurrence of these currents in the absence of externally applied current I suggested the following separation of i_m and V_m for the general case in which $I \neq 0$ (Lammel 1981*b*)

$$i_m = i_{m,I} + i_{m,J} \tag{9}$$

$$V_m = V_{m,I} + \Delta V_{m,J}. \tag{10}$$

These equations describe the membrane current as consisting of two components, (*a*) $i_{m,l}$, of local origin associated with a membrane potential level $V_{m,l}$, and (*b*) $i_{m,I}$, derived from the external current source related to a potential drop $\Delta V_{m,I}$. Because $i_{m,l}$ and $V_{m,l}$ are determined (*a*) by the size and distribution of the electromotive forces and (*b*) by the conductances in the trabecula, they must change as soon as the conductance distribution ($g_m[z]$) is altered by a voltage-clamp step (Fig. 3 of Lammel 1981*b*). This effect is clearly illustrated by the different shapes of the i_m distributions 1, 3, and 5 all computed for $I = 0$; however, each one is related to a different distribution $g_m(z)$. (For this special case $i_m = i_{m,l}$ and $V_m = V_{m,l}$.)

Fig. 5 shows results of the evaluation of nine of the twelve i_m profiles from which the $(i_t)_m$ vs V_m relation of Fig. 2 was constructed. To relate the current distributions to the currents determined experimentally, the current densities i_m, $i_{m,I}$ and $i_{m,l}$ were converted into currents I_m, $I_{m,I}$, and $I_{m,l}$ by integration with respect to length (z) and plotted against the clamp potential (membrane potential of the test section at $z = 0.25$ mm). Fig. 5 a shows the currents passing the cell membrane within the test compartment (curves α_1, β_1, and γ_1; integration interval $0 \leq z \leq 0.5$ mm), and Fig. 5 b shows those flowing through the membrane within the left-hand part of the sucrose compartment (curves α_2, β_2 and γ_2; integration interval $0.5 \leq z \leq 1.3$ mm, i.e., the region of $i_{m,I}$ exit or entrance, respectively). Without giving the details of the mathematical procedure applied to determine $i_{m,I}$ and $i_{m,l}$, we reproduce the steps of the preceding paper in the interpretation of Fig. 5. First, it is important to point out that curve α_1 in Fig. 5 a, which represents the total membrane current, I_m, of the test section, is very similar to the original membrane current-voltage curve (at $c_{Na,o} = c_{Na,T}$ and $c_{K,o} = c_{K,T}$), if I_m is referred to unit of membrane surface. Minor modifications, e.g., a shift of the positive reversal potential to the left by 5 mV, are caused by the nonuniformity of the external ion concentrations and of the membrane potential within the test section, i.e., of the two variables determining i_m (Eqs. 3–7). Modifications of the measured current-voltage relation (curve ϵ in the top panel) in regard to curve α_1 are due to the following effects. (*a*) Since $I_{m,I} = I_m - I_{m,l}$, the current component that passes from the test segment into the external circuit (curve β_1), differs from I_m (curve α_1) by the amount of the local circuit current of this section (curve γ_1); curve $\alpha_1 \rightarrow$ curve β_1 ($\beta_1 = \alpha_1 - \gamma_1$). (*b*) Current that flows through the cell membrane within the sucrose compartment (curve β_2) is included in the external current circuit; curve $\beta_1 \rightarrow$ curve δ ($\delta = \beta_1 + \beta_2$; $\beta_2 = \alpha_2 - \gamma_2$). (*c*) Part of the current I applied to the trabecula bypasses the cells as shunt current. This current adds to the measured membrane current ($\beta_1 + \beta_2$) and makes up the difference between curve ϵ and curve δ; curve $\delta \rightarrow$ curve ϵ (curve ϵ is a replot of curve $(i_t)_m$ of Fig. 2).

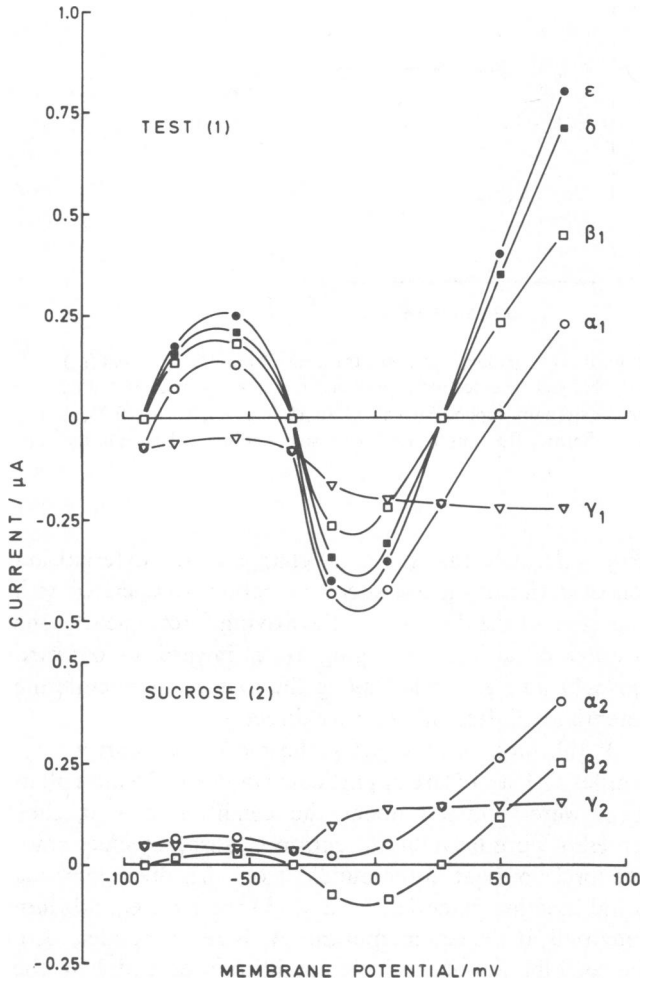

FIGURE 5 Current components of test compartment (top, 1) and of adjoining part of the sucrose compartment (bottom, 2) plotted against the membrane potential of the test section (clamp potential). The membrane current (O) in each of the two compartments (α_1 and α_2, respectively) is separated into current from the external current source (□; β_1 and β_2, respectively) and local circuit current (▽; γ_1 and γ_2, respectively): $\alpha_1 = \beta_1 + \gamma_1$; $\alpha_2 = \beta_2 + \gamma_2$. Curve δ (■), membrane current from test and sucrose region which flows through the external circuit: $\delta = \beta_1 + \beta_2$. Curve ϵ (●), measured current: $\epsilon = \delta$ + shunt current.

The variation of the local circuit current with the membrane potential (curves γ_1 and γ_2) again illustrates its dependence on the membrane conductance distribution along the model trabecula already mentioned. In the

voltage range, where the slow inward current channels become activated, there is a marked increase of this current component. (The incomplete amplitude match of the mirror fashioned curves, γ_1 and γ_2, indicates that the local circuit loop that passes the test section is not complete within the integration interval of the sucrose compartment.) Furthermore, we can see from the plot of the current components of the test section that the local circuit current causes the shift of both the measured resting potential and the positive reversal potential in a negative direction with respect to the related zero current potentials of curve α_1. The zero current potential in the negative slope range, on the other hand, is shifted to a more positive value by the flow of the local circuit current. Finally, note that, in contrast to the test section, the net membrane current, I_m, of the neighboring part of the sucrose segment (curve α_2) is outward at any clamp potential. This is due to the shift of the ionic equilibrium potentials in a negative direction according to the interstitial concentration distributions, which is associated with a reversal of the driving force for the slow inward current (see description of the current profiles of Fig. 4).

DISCUSSION

A central point in the analysis of sucrose gap operation is the modification of the measured current-voltage relation with regard to the true membrane current-voltage relation. The model underlying the present analysis simulates effects that produce such a modification. The current-voltage relationship considered is composed of two components, an outward background current (i_{bg}), which exhibits properties of inward-going membrane rectification, and an inward current, which represents the activated slow inward current (i_s) of cardiac muscle. The resulting current-voltage curve is N-shaped and crosses the zero current line at three different potentials.

Limitations of the Analysis

Before discussing the distorting effects on the current-voltage relation revealed by the computations, it is necessary to consider some inherent limitations. The membrane properties assumed for the model trabecula are not derived from methodically independent measurements, but from results obtained by the sucrose gap method itself; i.e., from results that are already distorted by the recording method analyzed. Therefore the distortions obtained cannot be regarded as describing the exact relationship between the measured and the true membrane current-voltage relation. Rather they must be considered as reflecting alterations that would occur if the membrane would have the conducting properties defined in Eqs. 3–7. The reason for choosing this description was that equations derived from independent (undistorted) measurements, which express the slow inward current in terms of intra- and extracellular ion concentrations and transmembrane voltage, were not available when setting up the model.

A similar reservation should be made when assessing possible interference of several time dependent processes with our simplifying approach of neglecting time variation of the membrane current. This simplification is based on experimental reports about time constants of activation (τ_d) and inactivation (τ_f) of the slow inward current and time constants of the charging current that flows after imposing a voltage-clamp step to the test section (τ_c). There is still considerable uncertainty about the kinetics of i_s in cardiac cells (e.g., Beeler and Reuter, 1977; McDonald, 1982). For the following arguments, we use the formulation by Beeler and Reuter (1977), because (*a*) this is the only complete analytic description for mammalian ventricular myocardium in the literature, and (*b*) it has been successfully applied in the simulation of the action potential of this tissue including a number of phenomena related to the voltage and time dependence of i_s.

(*a*) The reconstruction of the current-voltage relationship for the peak inward current from the respective potential and current distributions established at the time this peak value is reached, is reasonable only if these distributions are not contaminated by capacitive currents. This assumption seems justified on the following grounds. Results of several authors on mammalian trabeculae of different origin and geometry indicate that the capacitive current can be safely distinguished from the slow inward current by extrapolation methods, the average time constants reported ranging between 1.3 ms (Beeler and Reuter, 1970) and 5.4 ms (McGuigan, 1974) (others report 0.2–2ms [New and Trautwein, 1972]; 2.3–4 ms [time constant of the slower one of two components observed by McDonald and Trautwein, 1978]). Certainly, the time course of the capacitive current is not simply exponential (e.g., Jakobsson et al., 1975; Attwell and Cohen, 1977). However, the order of magnitude of these empirical values seems reasonable in consideration of the theoretical work by Schoenberg and Fozzard (1979) and Haas and Brommundt (1980), which includes the distributed resistance residing in the intercellular clefts; even if the analysis by these authors does not allow conclusions to be drawn about the contribution of the charging of the membrane surface in the sucrose compartment. On the other hand, computing the time course of i_s at different clamp potentials (between -55 and $+100$ mV) by integration of Eqs. 10–13 of Beeler and Reuter (1977) shows that the peak value of this current is reached between 55 and 145 ms, i.e., at times that are at least ten times longer than the time constant of the capacitive current.

(*b*) The procedure by which the mathematical description of the membrane current has been simplified only provides a close replica of the peak inward current if the time constant of inactivation is very long compared to the activation time. Only in this case can the activation variable (*d*) be assumed to closely reach its steady-state

value (d_∞) at the time of peak inward current (as implied by Eqs. 5 and 6). On the basis of the formulation by Beeler and Reuter (1977) this assumption can be taken as a rough approximation only; this is to say, some not negligible inactivation must be expected to proceed causing the inward current to reach its peak value before d reaches d_∞. In fact, this means that the current calculated from Eqs. 5 and 6 at a given membrane potential is somewhat larger than the peak inward current obtained when using the same formulation of d_∞ and f_∞, but taking into account the time variation of these variables. The difference between these two current values can also be assessed by means of the current traces computed from Eqs. 10–13 of Beeler and Reuter (1977). It is largest in the potential range between −30 and 0 mV, where it amounts to some 30%. Outside of this range it leans towards values of ~10%, both with decreasing and increasing membrane potentials. Taking these differences into account would quantitatively modify our results but not change the main conclusions.

(*c*) If the slow inward current is predominantly carried by calcium ions, some effect on the measured current must also be expected to arise from concentration changes due to the flux of this ions across the cell membrane. Variations of the intracellular Ca concentration during the clamp pulse associated with the transmembrane flux are disregarded; for, the magnitude and time course of such variations close to the cell membrane are the result of the interference of this flux with several other processes, like intracellular movement (diffusion), binding to proteins, release from and uptake into intracellular stores and are therefore not well known in quantitative terms. Qualitatively, an increase of the internal Ca concentration would produce an alteration of the calcium current-voltage relation towards the one calculated under the assumption that i_s is carried by sodium ions and may therefore be estimated by comparison of the different curves illustrated in Fig. 3. (not considering secondary effects of internal [Ca] on membrane permeabilities other than for Ca ions). To obtain an upper estimate of concentration changes in the intercellular fluid spaces caused by the transmembrane Ca flux, we calculate the overall change that would occur in a plane sheet representing a cleft between two adjacent cells (but bounded by an infinite area of cell membrane on either side) if the maximum inward current, flowing at a clamp potential of ~ −10 mV, would constantly flow for a time period of 100 ms (i.e., about the time of i_s to reach its peak value). Taking the cleft width as 1 μm (Johnson and Lieberman, 1971) and the current density as 10 μA/cm^2 (Beeler and Reuter, 1977; Reuter and Scholz, 1977), this concentration change comes to 0.1-mmol/l cleft volume. A change of this size, which amounts to some 5% of the physiological extracellular concentration (1.8 mmol/l), is probably too small to significantly influence the axial current distribution; particularly, because the current density within the sucrose compartment is predicted to be appreciably smaller than 10 μA/cm^2 (see profiles in Fig. 4 d). (An almost identical estimate of the concentration change is obtained considering an infinite volume of ventricular tissue and using the morphological data surface per volume and ρ as given in the Model section.)

Distortions of the Current-Voltage Relation

The conclusions that can be drawn with regard to the determination of the N-shaped current-voltage relation concern both the values of the zero current (reversal) potentials and the size of the measured current. The resting potential and the positive reversal potential are predicted more negative than their corresponding values on the membrane current-voltage curve, whereas the reversal potential in the range of negative slope conductance is shifted to a more positive value. Of the three zero current potentials, the positive reversal potential is affected the most.

While the shifts of the zero current potentials may be attributed purely to the effect of local circuit currents, there are two further current components that contribute to the modification of the current amplitude; (*a*) a shunt current that bypasses the cells altogether, and (*b*) a fraction of externally applied current that flows through cell membrane areas within the sucrose compartment. It is immediately evident and has already been analyzed by means of the linear cable theory (see Appendix of McGuigan [1974] written by Tsien and McGuigan) that, regardless of the current direction, these two current components tend to increase the measured current by comparison with the membrane current of the test section. Therefore, the present result that inward currents may be measured too low by the sucrose gap technique is unexpected and emphasizes the effect of local circuit currents illustrated in Fig. 5. Computations not included in the Results section showed that even when the shunt factor was increased threefold (R_i/R_e changed from 0.085 to 0.255 by increasing R_i, other conditions as in Fig. 2), the maximal net inward current (at $V_m = -10$ mV) was still underestimated by 14%. Note that the positive reversal potential of the measured curve was almost unchanged by this procedure (shift by −0.9 mV), a result that is in line with the very small effects on the resting potential obtained previously by variation of the internal resistance (Fig. 9; Lammel, 1981*b*). In the case of outward currents, the present results resemble those of the preceding paper (Lammel, 1981*b*) in showing that, for these currents, the local circuit current represents an important factor contributing to an overestimation.

Measurements of reversal potentials have been crucial for identifying ion species that carry particular membrane current components. The fact that the reversal potential of the slow inward current in mammalian ventricular myocardium was found to be much less positive than would be

predicted from the intra- and extracellular calcium concentrations, despite other evidence that indicates that this current is predominantly carried by calcium ions, this fact has been the subject of both theoretical consideration and experimental work (for review, see Reuter, 1973). Bassingthwaighte and Reuter (1972) interpreted their results by assuming that the calcium concentration in a limited space, close to the inner surface of the cell membrane, was higher than the free calcium concentration in the myoplasm. More recently, Reuter and Scholz (1977) explained the low reversal potential of i_s in cow ventricular trabeculae on the basis of the permeability ratio of the conductance channel for calcium, sodium, and potassium. The relative permeabilities used by these authors to fit their results ($P_{Ca}/P_{Na} = P_{Ca}/P_K = 100$) were adopted for one set of computations of the present study. From the results based on this assumption (Fig. 3 *c*), we may conclude that the selectivity of the i_s channel for Ca and/or Na ions, in regard to its permeability for K ions, is higher than calculated from the reversal potentials measured with the sucrose gap technique. (Note, in this connection, that because of much higher absolute concentrations of Na and K, these ions are predicted to participate appreciably in the total current flow, in spite of high selectivity of the channel for Ca ions. Reuter and Scholz [1977] calculated that, at physiological outside concentrations, ~ one-third of the ions carrying inward current in cow trabeculae [at $V_m = -10$ mV] are Na ions.)

In view of the recent discussion of general problems involved in the determination of i_s, we consider the methodical errors analyzed here in regard to some sources of error that are unrelated to the recording technique. Two aspects of these general problems may be distinguished. First, as already stated in the Results section, the evaluation of i_s rests on methods to separate this current from outward currents. Efforts made so far to eliminate i_s, either by application of blocking substances or by withdrawal of the external ion that is thought to carry this current, seem to affect currents through potassium channels as well, and therefore introduce uncertainty into quantitative assessments. (For more detailed discussion on this point, see Hagiwara and Byerly [1981]; for experimental evidence Kass and Tsien [1975] and Nawrath et al. [1977].) Similarly, graphical methods, frequently applied to evaluate i_s, depend on the validity of assumptions made about the outward current. Moreover, these methods are unsuitable for determining the absolute size of i_s for membrane potential levels at which the conductance system of this current is not totally inactivated. (For a recent account of these problems, see Coraboeuf [1980].) In the present investigation, we supposed that i_s can principally be separated from other currents by elimination of i_s. The basic (qualitative) features of the methodical distortions under study, however, seem to be independent of this assumption and must be expected to superimpose themselves on errors due to incomplete selectivity or secondary effects of methods employed to separate the different current components.

An interesting result obtained when simulating the experimental subtraction protocol to evaluate i_s is that errors from the same origin, which occur in the measurement of two currents, may cancel each other to some extent. On the basis of the interpretation of the distorting effects given in connection with Fig. 5, this can be explained as follows. Because the local circuit current was defined as being caused exclusively by electromotive forces present in the model trabecula, its acting direction is independent of the direction of externally applied current I. This means that in the measurement of both net inward and outward current, the local circuit current acts as an inward component within the test section (Fig. 5; this paper and Fig. 7 *A*; Lammel, 1981*b*). Therefore, it is partially cancelled when the outward current $(i_{bg})_m$ is subtracted from the net inward current $(i_t)_m$, so that the pure inward current $(i_s)_m$ is obtained. Apart from the two other current components contributing to the distortion (shunt current and externally applied current passing the cell membrane within the sucrose compartment), there is no complete cancellation of errors, because the size of the local circuit current depends on the membrane conductance distribution along the trabecula. However, the conductance distributions for the two measured current-voltage relations are different at any clamp potential that is high enough to activate i_s.

The second problem of general relevance is related to the high asymmetry of the calcium concentration between the two sides of the cell membrane. This creates a unique situation for current carried by this ion. As pointed out by Hagiwara and Byerly (1981) and as apparent by inspection of Fig. 3 *B*b, Ca current-voltage relations, which describe the movement of ions between regions with concentrations that differ by a factor of 10^5, are predicted to be highly nonlinear. At membrane potentials above + 60 mV, the Ca current becomes so small that its reversal potential appears to be essentially unmeasurable by electrical methods (particularly, in view of the uncertainty mentioned, which is inherent to the separation of the currents). This major aspect remains unaffected by the present results. A comparison between the different current-voltage curves of Fig. 3 *B* indicates that the shift of the Ca reversal potential due to the distorting effects is about the same, both in size and direction, as for the other two cases simulated. But, within the range of membrane potential, which must be evaluated to determine the reversal potential, the curve representing the measured calcium current-voltage relation is almost undiscernable from the original current-voltage curve.

I am indebted to Dr. R. Niedergerke, Department of Biophysics, University College London, for much help during the initial stages of this work.

Received for publication 23 December 1981 and in final form 22 December 1982.

REFERENCES

Attwell, D., and I. Cohen. 1977. The voltage clamp of multicellular preparations. *Prog. Biophys. Mol. Biol.* 31:201–245.

Bassingthwaighte, J. B., and H. Reuter. 1972. Calcium movements and excitation-contraction coupling in cardiac cells. *In* Electrical Phenomena in the Heart. W. C. De Mello, editor. Academic Press Inc., New York. 353–395.

Beeler, G. W., and H. Reuter. 1970. Voltage clamp experiments on ventricular myocardial fibres. *J. Physiol. (Lond.).* 207:165–190.

Beeler, G. W., and H. Reuter. 1977. Reconstruction of the action potential of ventricular myocardial fibres. *J. Physiol. (Lond.).* 268:177–210.

Bulirsch, R., and J. Stoer. 1966. Numerical treatment of ordinary differential equations by extrapolation methods. *Num. Math.* 8:1–13.

Coraboeuf, E. 1980. Voltage clamp studies of the slow inward current. *In* The Slow Inward Current and Cardiac Arrhythmias. D. P. Zipes, H. C. Bailey, and V. Elharrar, editors. Martinus Nijhoff, The Hague, Boston, London. 25–95.

Ellis, D. 1977. The effects of external cations and ouabain on the intracellular sodium activity of sheep heart Purkinje fibres. *J. Physiol. (Lond.).* 273:211–240.

Goldman, D. E. 1943. Potential, impedance and rectification in membranes. *J. Gen. Physiol.* 27:37–60.

Haas, H.G., and G. Brommundt. 1980. Influence of intercellular clefts on potential and current distribution in a multifiber preparation. *Biophys. J.* 30:327–350.

Hagiwara, S., and L. Byerly. 1981. Calcium channel. *Annu. Rev. Neurosci.* 4:69–125.

Hodgkin, A. L., and P. Horowicz. 1959. The influence of potassium and chloride ions on the membrane potential of single muscle fibres. *J. Physiol. (Lond.).* 148:127–160.

Hodgkin, A. L., and A. F. Huxley. 1952*a*. Currents carried by sodium and potassium ions through the membrane of the giant axon of Loligo. *J. Physiol. (Lond.).* 116:449–472.

Hodgkin, A. L., and A. F. Huxley. 1952*b*. The components of membrane conductance in the giant axon of Loligo. *J. Physiol. (Lond.).* 116:473–496.

Hodgkin, A. L., and B. Katz. 1949. The effect of sodium ions on the electrical activity of the giant axon of the squid. *J. Physiol. (Lond.).* 108:37–77.

Hutter, O. F., and D. Noble. 1960. Rectifying properties of heart muscle. *Nature (Lond.).* 188:495.

Jakobsson, E., L. Barr, and J. A. Connor. 1975. An equivalent circuit for small atrial trabeculae of frog. *Biophys. J.* 15:1069–1085.

Johnson, E. A., and M. Lieberman. 1971. Heart: excitation and contraction. *Annu. Rev. Physiol.* 33:479–532.

Kass, R. S., and R. W. Tsien. 1975. Multiple effects of calcium antagonists on plateau currents in cardiac Purkinje fibers. *J. Gen. Physiol.* 66:169–192.

Katz, B. 1949. Les constantes électriques de la membrane du muscle. *Arch. Sci. Physiol.* 3:285–300.

Keenan, M. J., and R. Niedergerke. 1967. Intracellular sodium concentration and resting sodium fluxes of the frog heart ventricle. *J. Physiol. (Lond.).* 188:235–260.

Lammel, E. 1981*a*. A theoretical study on the sucrose gap technique as applied to multicellular muscle preparations. I. Saline-sucrose interdiffusion. *Biophys. J.* 36:533–553.

Lammel, E. 1981*b*. A theoretical study on the sucrose gap technique as applied to multicellular muscle preparations. II. Methodical errors in the determination of outward currents. *Biophys. J.* 36:555–573.

Lee, C. O., and H. A. Fozzard. 1975. Activities of potassium and sodium ions in rabbit heart muscle. *J. Gen. Physiol.* 65:695–708.

Marceau, F. 1904. Recherches sur la structure et le développement comparés des fibres cardiaques dans la série des vertébrès. *Annes. Sci. Nat. (Zool.).* 1904:191–365.

McDonald, T. F. 1982. The slow inward current in the heart. *Annu. Rev. Physiol.*44:425–434.

McDonald, T. F., and W. Trautwein. 1978. Membrane currents in cat myocardium: separation of inward and outward components. *J. Physiol. (Lond.).* 274:193–216.

McGuigan, J. A. S. 1974. Some limitations of the double sucrose gap, and its use in a study of the slow outward current in mammalian ventricular muscle. *J. Physiol. (Lond.).* 240:775–806.

Nawrath, H., R. E. Ten Eick, T. F. McDonald, and W. Trautwein. 1977. On the mechanism underlying the action of D-600 on slow inward current and tension in mammalian myocardium. *Circ. Res.* 40:408–414.

New, W., and W. Trautwein. 1972. Inward currents in mammalian myocardium. *Pflügers Arch. Eur. J. Physiol.* 334:1–23.

Page, E., and L. P. McCallister. 1973. Quantitative electron microscopic description of heart muscle cells. Application to normal, hypertrophied and thyroxin-stimulated hearts. *Am. J. Cardiol.* 31:172–181.

Page, S. G., and R. Niedergerke. 1972. Structures of physiological interest in the frog heart ventricle. *J. Cell. Sci.* 11:179–203.

Reuter, H. 1973. Divalent cations as charge carriers in excitable membranes. *Prog. Biophys. Mol. Biol.* 26:1–43.

Reuter, H. 1979. Properties of two inward membrane currents in the heart. *Annu. Rev. Physiol.* 41:413–424.

Reuter, H., and H. Scholz. 1977. A study of the ion selectivity and the kinetic properties of the calcium dependent slow inward current in mammalian cardiac muscle. *J. Physiol. (Lond.).* 264:17–47.

Schoenberg, M., and H. A. Fozzard. 1979. The influence of intercellular clefts on the electrical properties of sheep cardiac Purkinje fibers. *Biophys. J.* 25:217–234.

Weidmann, S. 1970. Electrical constants of trabecular muscle from mammalian heart. *J. Physiol. (Lond.).* 210:1041–1054.